Journal of Contaminant Hydrology 251 (2022) 104079

Contents lists available at ScienceDirect

Journal of Contaminant Hydrology

journal homepage: www.elsevier.com/locate/jconhyd

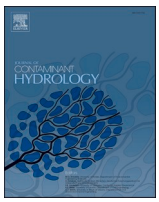

Experimental and numerical investigation of the effect of temporal variation in ionic strength on colloid retention and remobilization in saturated porous media

Yerramilli Sai Rama Krishna [a], N. Seetha [a,*], S. Majid Hassanizadeh [a,b,c]

[a] Department of Civil Engineering, Indian Institute of Technology Hyderabad, Kandi, Sangareddy 502284, India
[b] Stuttgart Center for Simulation Science (SIMTECH), Integrated Research Training Group SFB 1313, Stuttgart University, Germany
[c] Department of Earth Sciences, Utrecht University, 3584, CB, Utrecht, the Netherlands

ARTICLE INFO

Keywords:
Colloids
Transients
Ionic strength
Remobilization
Porous media
Modeling

ABSTRACT

Temporal variations in the chemistry of infiltrating water into the subsurface are known to cause remobilization of colloids from the grain surfaces, thereby increasing the travel distance of the colloidal contaminants. Hence, it is essential to thoroughly understand the transport, deposition, and release mechanisms of colloids in the subsurface, through laboratory experiments and modeling. There are only a few experiments in which the chemistry of inflow water is changed rapidly during colloid transport. Also, although some models have been presented for simulating the effect of transient chemistry on the fate of colloids, there is no consensus in this regard, as the proposed models suffer from shortcomings. In this study, we systematically investigated the effect of temporal variations in ionic strength on the remobilization of deposited colloids in saturated porous media through laboratory column experiments and numerical modeling. Four sets of column experiments were performed, in which we injected carboxylate-modified latex colloids at a given ionic strength for a specified period. After breakthrough of colloids, the ionic strength of inflowing water was decreased in a stepwise manner to 0 mM (DI water). The initial ionic strength values of the four experiments were 100, 50, 25, and 10 mM. We observed partial release of deposited colloids after several steps of ionic strength decrease with significant release observed only when the ionic strength was reduced to below 10 mM. We also found that the fraction of released colloids decreased with increasing value of initial ionic strength of inflow water. We have developed a mathematical model incorporating a novel formulation for ionic strength-dependent deposition and release. The model is found to capture the colloid breakthrough curves reasonably well for all experiments with the same set of parameter values, except the one at the initial ionic strength of 25 mM.

Introduction

Groundwater is the major source of drinking water for the majority of rural and urban population (Carrard et al., 2020). Colloidal particles such as silica, clays and metal oxides are naturally present in the subsurface. Apart from this, colloidal contaminants such as pathogenic microorganisms and engineered nanoparticles enter the subsurface through various anthropogenic activities (Powelson et al., 1993; Bundschuh et al., 2018). Rapid infiltration due to rain events and artificial recharge of groundwater cause physical and chemical perturbations in the subsurface. These lead to the colloids previously deposited on soil surface to get remobilized, causing recontamination of the groundwater resources. Hence, it is necessary to understand the colloid transport, deposition and remobilization mechanisms in the subsurface to protect drinking water wells from contamination.

Colloid deposition mechanisms in porous media are usually studied using packed soil-columns in the laboratory. Numerous studies on colloid transport are reported in the literature in which experiments were performed under steady-state flow and constant chemistry conditions (Elimelech and O'Melia, 1990; Sadeghi et al., 2011; Wan and Wilson, 1994; Wang et al., 2012). Colloid transport models under steady state-flow and chemistry conditions have been around for a long time and are straight forward (Bradford and Bettahar, 2005; Li and Johnson, 2005; Sasidharan et al., 2017; Syngouna and Chrysikopoulos, 2011; Torkzaban et al., 2008). They include terms for advection, dispersion, attachment, detachment and straining. Some complications such as

* Corresponding author.
E-mail address: seetha@ce.iith.ac.in (N. Seetha).

https://doi.org/10.1016/j.jconhyd.2022.104079
Received 26 May 2022; Received in revised form 27 August 2022; Accepted 12 September 2022
Available online 16 September 2022

aggregation kinetics can be added (Katzourakis and Chrysikopoulos, 2021). However, an important phenomenon is temporal variations in chemistry which significantly affects colloid transport behavior. A relatively lesser number of studies have dealt with the effect of (temporal) variations in chemistry on colloid remobilization and deposition in porous media (some examples are: Bradford et al., 2015; Cheng and Saiers, 2009; Lenhart and Saiers, 2003; Torkzaban et al., 2015; Tosco et al., 2009; Wang et al., 2014; Sadeghi et al., 2013). Experimental studies have observed a spike release of colloids from soil due to decrease in ionic strength beyond a threshold value (Bradford et al., 2012; Lenhart and Saiers, 2003; Tosco et al., 2009; Torkzaban et al., 2010). Sadeghi et al. (2013) found that a spike release of colloids occurred even though the ionic strength was constant but calcium ions were replaced with sodium ions. Colloid deposition and release from the grain surface is governed by colloid-soil interaction forces. Transients in chemistry results in changes in interaction energy which promotes release of attached colloids. For example, decreases in ionic strength increases the energy barrier between the colloids and solid surface, resulting in detachment of attached colloids from soil grains (Fang et al., 2013; Johnson et al., 2010; Torkzaban et al., 2007).

Colloid release under transient chemistry conditions is simulated by coupling the governing equations for colloid transport and solution chemistry. The effect of chemistry has been taken into account by assuming the colloid detachment rate coefficient to be an empirical function of solution chemistry (Lenhart and Saiers, 2003; Tosco et al., 2009) or using models with a one adsorption site (equilibrium or kinetic) or two adsorption sites (equilibrium and kinetic or two kinetic) (Bradford et al., 2012; Bradford et al., 2015). Lenhart and Saiers (2003) assumed heterogeneous colloidal population and modelled colloid release by dividing the immobile colloidal phase into a number of compartments, each compartment releasing colloids at its own critical salt concentration. The model performance was evaluated by fitting the breakthrough curves obtained from experiments in which the ionic strength was reduced in a stepwise manner from an initial ionic strength of 100 mM to 0 mM (DI water). A good match between the simulated and experimental results was observed. However, when the estimated parameters at an initial ionic strength of 100 mM were used to predict the colloid release curves obtained from experiments with initial ionic strengths of 40 mM and 10 mM, the model overestimated the release peaks (for 10 mM initial ionic strength) and the declining limb of breakthrough curves (for initial ionic strengths of 40 mM and 10 mM). Tosco et al. (2009) coupled dual-site colloid and solute transport models with the attachment and detachment rate coefficients expressed as empirical functions of ionic strength through critical deposition and release concentrations. They performed several sets of experiments with different initial ionic strengths and the subsequent release of the colloids was initiated by decreasing the ionic strength to 0 mM (DI water). Since all experiments were performed at the same physicochemical conditions except the difference in the initial ionic strength, one would expect model parameters, including the critical deposition and release ionic strengths, to remain the same. However, they fitted different experimental sets separately (in order to obtain a good fit between observed and simulated data), and thus obtained different sets of parameter values for different experiments. Bradford et al. (2012) developed a dual permeability model for colloid transport and release under transient ionic strength conditions, in which the detachment term was mechanistically modelled based on a balance of hydrodynamic and adhesive torques. Bradford et al. (2015) developed equilibrium, kinetic and combined equilibrium and kinetic models to describe colloid release under transient ionic strength or pH conditions. They linked the amount of colloid release to the fractional solid surface area that contributed to retention, where the fractional solid surface area was estimated experimentally from mass balance information. However, they use different functions for colloid release for different boundary conditions and the mechanisms during steady-state and transient chemical conditions were treated independent of each other. Also, this model did not account for the re-deposition of remobilized colloids. The foregoing short review of the literature indicates that further research is needed to develop a model that is valid under a variety of conditions without re-estimating the model parameter values.

The objectives of this study are: a) to develop a mathematical model that is capable of simulating the fate of colloids in saturated porous media, when there are temporal variations in ionic strength, for a wide range of ionic strengths, with a consistent set of parameter values, and b) to systematically evaluate the performance of the model through comparison with experiments. Four sets of column experiments were performed in which colloids were deposited at four different ionic strengths, followed by decreasing the ionic strength in a stepwise manner at the column inlet to 0 mM. The experimental data was further simulated using a mathematical model which accounted for ionic-strength dependent colloid deposition and release.

2. Materials and methods

2.1. Porous medium, colloids and background electrolyte

Natural river sand with grain size between 425 and 600 μm, representative of sandy aquifers (Bales et al., 1997; Tan et al., 1994), was used as the porous medium for performing column experiments. The sand was acid washed prior to packing it into the column to remove metal oxides and organic impurities from the grain surface. Acid washing involved the following sequential steps (Kohler et al., 1996; Sasidharan et al., 2014): soaking the sand in 37% HCl for three days, washing with DI water, and then washing in NaOH for 2 h in a shaker. After this, the sand was thoroughly rinsed with DI water and oven-dried at $105^{\circ}C$ for 5 h. The efficiency of the acid washing procedure in removing the metal oxides and organic impurities was determined by analyzing the sand samples before and after acid treatment using inductively coupled plasma mass spectrometry. The detailed procedure for determining the metal content of the sand is given in appendix A1.

Carboxylate-modified latex (CML) beads of size 1 μm (Thermo Fisher Scientific Pvt. Ltd.) were used as colloidal particles in this study. Sodium chloride was used for preparing background electrolyte at various ionic strengths of 100, 50, 25, 10, 1, and 0.1 mM. pH of the background electrolyte was adjusted to 7 by addition of 0.1 N HCl and 0.1 M NaOH. Injection colloidal suspension of concentration 7.3×10^{7} no./mL was prepared by diluting the stock in the background electrolyte at the desired ionic strength. The colloidal suspension was sonicated for 20 min in an ultra sonicator (Branson ultrasonics) before injecting it into the column to ensure a uniform dispersion of colloids. The zeta potentials of CML colloids and sand at various ionic strengths were measured using a Zeta sizer (Malvern analytical instruments). The zeta potential of the sand was measured after crushing it into fine powder and suspending it in the background electrolyte (Bergendahl and Grasso, 1999; Treumann et al., 2014).

2.2. Column experiments

Column experiments were performed in acrylic columns with 2.5 cm inner diameter and 15 cm length. The top and bottom ends of the column were equipped with stainless steel meshes to prevent the entry of sand into the inlet and outlet pipes and to maintain a uniform distribution of flow throughout the cross-section of the column. The column was placed vertically and wet packed with acid-washed sand in increments of 1 cm, along with tapping from the sides to maintain a tight, uniform packing of solid grains. The porosity and bulk density of the sand were measured to be 0.37 and 1.67 g/cm^3, respectively. The bottom end of the column was connected to a peristaltic pump which maintained a constant upflow rate of 1 mL/min throughout the experiment. It is known that the column orientation and hence, gravity has an important role in colloid deposition, with particle deposition rates being greater in the up-flow than in the down-flow direction (Chrysikopoulos

and Syngouna, 2014). However, the density of CML colloids (1.055 g/cm^3) is similar to that of water, and hence, the gravity effects can be considered negligible in this study.

The packed column was flushed with ten pore volumes (PVs) of DI water. Additional experiments described below show that natural colloids were not present in the effluent. After this, a tracer experiment was performed by passing 3 PVs of 100 mM NaCl, followed by 3 PVs of DI water. Effluent samples were collected from the column outlet at 6-min intervals and analyzed for NaCl concentration using an electrical conductivity meter. Next, the sand-packed column was equilibrated with background electrolyte at the desired ionic strength for 10 PVs. Finally, colloid transport experiments were performed. Each colloid transport experiment consisted of three stages: stages 1 & 2 correspond to transport under steady-state chemistry condition at a constant ionic strength, whereas stage 3 corresponds to transient chemistry conditions due to a step decrease in the ionic strength of the inflowing solution. In stage 1 (colloid deposition under steady-state chemistry condition), the inflow solution had a constant ionic strength and colloid concentration. Colloidal suspension in the reservoir was stirred frequently to prevent particle aggregation and settling. After exactly three pore volumes, in stage 2 (colloid elution under steady-state chemistry condition), the inflow was switched to a colloid-free solution without any change of flow rate and ionic strength. In stage 3 (transient chemistry), the ionic strength of inflow solution was decreased in a stepwise manner to DI water (0 mM) without any change of the flow rate. Each step-decrease in ionic strength was applied for 3 PVs except for the last step for which several PVs of DI water was applied. Effluent samples were collected from the column outlet at 6-min intervals and analyzed for colloid concentration using turbidity meter. Four sets of transient experiments (1, 2, 3 & 4) were performed in this study, each corresponding to a different initial ionic strength in stages 1 & 2 as given in Table 1. For example, experiment 1 was performed at an ionic strength of 100 mM in stages 1 & 2, followed by a stepwise sequential reduction in ionic strength to 50 mM, 25 mM, 10 mM, 1 mM, 0.1 mM and 0 mM (DI water) in stage 3.

In addition to the above four experiments, which involved all three stages, experiments 5, 6 and 7 were performed at stages 1 and 2 only (Table 1) at ionic strengths of 1 mM, 0.1 mM and 0 mM (DI water), respectively, to understand the colloid deposition behavior under constant chemistry at these ionic strengths. Each experiment was repeated three times to check the reproducibility of the experimental results. The above set of four release experiments was also performed, including all three stages but in the absence of CML colloids, to measure the release of natural colloids from the soil grains during transient chemistry conditions. We did not find any natural colloids leaching from the soil into the effluent.

Finally, three additional experiments were performed in which we measured the colloid retention profile along the soil column (experiments 8a, 8b, and 8c in Table 1). This was done for an initial ionic strength of 50 mM at the following stages: at the end of stage 2 (experiment 8a), after three step decreases of ionic strength from 50 mM to 1 mM (experiment 8b), and after four step decreases of ionic strength from 50 mM to 0.1 mM (experiment 8c). Each of the above trials consisted of dissecting the soil inside the column at the end of the experiment into approximately 1 cm long sections. The mass of colloids retained on the sand in each section was then determined by first adding 20 mL of DI water to sand followed by gentle shaking to release the colloids into the suspension (Bradford et al., 2007; Torkzaban et al., 2008). The suspension was then allowed to stand for 15 min for the sand particles to settle. After that, the colloid concentration in the supernatant was measured. Colloid retention profile is then plotted as the mass of colloids retained per mass of soil in each section versus distance from the inlet.

Table 1
List of column experiments performed in this study.

Experiment	Ionic strength, I (mM)						
	Stages 1 and 2	Stage 3					
		Step 1	Step 2	Step 3	Step 4	Step 5	Step 6
1	100	50	25	10	1	0.1	0
2	50	25	10	1	0.1	0	–
3	25	10	1	0.1	0	–	–
4	10	1	0.1	0	–	–	–
5	1	–	–	–	–	–	–
6	0.1	–	–	–	–	–	–
7	0	–	–	–	–	–	–
8a	50	–	–	–	–	–	–
8b	50	25	10	1	–	–	–
8c	50	25	10	1	0.1	–	–

2.3. Interaction energy calculation

The total interaction energy between colloid and grain surface was calculated using DLVO theory (Derjaguin and Landau, 1941; Verwey and Overbeek, 1948) as the sum of London van der Waals energy, electrostatic double-layer energy and Born repulsion energy assuming a sphere-plate interaction (Ryan and Elimelech, 1996). The total interaction energy, (Φ_{DLVO}), between colloid and grain surface is given as

$$\frac{\Phi_{DLVO}}{k_B T} = \frac{\Phi_{vdW}}{k_B T} + \frac{\Phi_{EDL}}{k_B T} + \frac{\Phi_{Born}}{k_B T} \tag{1}$$

where Φ_{vdW} [ML^{2}T^{-2}] is the van der Waals energy, Φ_{EDL}[ML^{2}T^{-2}] is electrostatic double-layer energy, Φ_{Born}[ML^{2}T^{-2}] is the Born repulsion energy, k_B[ML^{2}T^{-2}K^{-1}] is Boltzmann constant, and T [K] is temperature. The van der Waals energy was calculated using the expressions given by Gregory (1981) and Weroński and Elimelech (2008). The electrostatic double-layer energy and Born repulsion energy were calculated using expressions given by Hogg-Healy-Fuerstenau (Hogg et al., 1966) and Ruckenstein and Prieve (1976), respectively. The detailed description of the calculation of van der Waals energy, electrostatic double-layer energy, and Born repulsion energy are given in appendix A2.

3. Mathematical model

3.1. Governing equations

The ionic strength variation in the column (during stage 3) was simulated by solving one-dimensional advection-dispersion equation as follows:

$$\frac{\partial I}{\partial t} = D_L \frac{\partial^2 I}{\partial z^2} - \bar{v}\frac{\partial I}{\partial z} \tag{2}$$

where, I [Molar] is ionic strength, D_L [L^2T^{-1}] is the dispersion coefficient, and $\bar{v}$ [LT^{-1}] is the average pore-water velocity. Colloid transport was simulated by one-dimensional advection-dispersion equation modified to account for deposition and release as:

$$\frac{\partial c}{\partial t} + \frac{\rho_b}{\theta}\frac{\partial s}{\partial t} = D_L \frac{\partial^2 c}{\partial z^2} - \bar{v}\frac{\partial c}{\partial z} \tag{3}$$

where, c [ML^{-3}] is colloid concentration in aqueous phase, ρ_b [ML^{-3}] is the bulk density of soil, θ [−] is the porosity of soil and s [MM^{-1}] is the mass fraction of colloids attached to soil grains. During the preliminary fitting of the colloid breakthrough data from stages 1 and 2 of experiments 1–7, we tried various models including one-site kinetic model, and two-site kinetic model with site-1 being reversible and site-2 being irreversible. We found that the two-site kinetic model with reversible deposition at site-1 and irreversible deposition at site-2 fitted the data well. However, the values of attachment and detachment rate

coefficients for site 1 were very large, which indicates that site-1 is a fast or equilibrium site and site-2 is a slow or kinetic site. So, the colloid deposition on the grain surface was described using a two-site model (Eqs. (4a)-(4c)) with sites 1 and 2 representing equilibrium and kinetic sites, respectively. This model gave the same fitting as that of the two-site kinetic model. Moreover, we assume that the colloids attached to the kinetic sites are affected by the change of ionic strength (during stage 3). The governing equations for adsorption are:

$$s_1 = fk_D c \tag{4a}$$

$$\frac{\rho_b}{\theta}\frac{\partial s_2}{\partial t} = (1-f)k_a c - \frac{\rho_b}{\theta}k_d s_2 - \frac{\rho_b}{\theta}k_d' H_0\left(\frac{\partial I}{\partial t}\right)s_2 \tag{4b}$$

$$s = s_1 + s_2 \tag{4c}$$

Here, s_1 [MM^{-1}] is the mass fraction of colloids attached to site 1 (mass of colloids attached to site 1 per unit mass of dry soil), s_2 [MM^{-1}] is the mass fraction of colloids attached to site 2 (mass of colloids attached to site 2 per unit mass of dry soil), f [−] is the fraction of sites in equilibrium with the liquid phase, k_D [$M^{-1}L^3$] is the equilibrium distribution coefficient, k_a [T^{-1}] and k_d [T^{-1}] are the rate coefficients of attachment and detachment of colloids to the kinetic site, k'_d [T^{-1}] is the rate coefficient for the release of colloids from kinetic site during transients in ionic strength, and $H_0\left(\frac{\partial I}{\partial t}\right)$ is the Heaviside step function defined as

$$H_0\left(\frac{\partial I}{\partial t}\right) = \begin{cases} 1; \dfrac{\partial I}{\partial t} < 0 \\ 0; \dfrac{\partial I}{\partial t} \geq 0 \end{cases} \tag{5}$$

The colloid release rate coefficient during transients in ionic strength was expressed as $k'_d = \frac{k'_{d_0}}{1+\left(\frac{I}{I_c}\right)^{\beta}}$, where k'_{d_0}[T^{-1}] is the maximum value of release rate coefficient which occurs at zero ionic strength, I_c [Molar] is the critical ionic strength below which the release is fast, and β [−] is a constant (Tosco et al., 2009). We observed from stages 1 and 2 of experiments 1–7 that the values of the rate coefficients,k_D, k_a, k_d and f depend on ionic strength. Coefficients k_a and k_D were found to increase with increase in ionic strength whereas k_d and f decrease with increase in ionic strength. Hence, the colloid deposition parameters change during transients in ionic strength (stage 3), and therefore it is important to account for the effect of ionic strength variation on colloid deposition parameters in the model. We tried various functions for relating k_D, k_a, k_d and f to ionic strength, and found the following formulas to give us the best fit:

$$k_D = a_1 I^2 + a_2 I + a_3 \tag{6}$$

$$k_a = b_1 I^2 + b_2 I + b_3 \tag{7}$$

$$k_d = d_1 exp(-d_2 I) \tag{8}$$

$$f = e_1 exp(e_2 I) \tag{9}$$

where, a_i, b_i, c_j, and d_j ($i = 1, 2, 3$, and $j = 1, 2$) are the coefficients whose values were estimated from the experimental data given in Table 3. Eqs. (2)–(9) represent the complete set of equations governing the transport of colloids in porous media. They were solved by imposing the following initial and boundary conditions.

$$I(z,0) = I_0, c(z,0) = s_1(z,0) = s_2(z,0) = 0 \tag{10}$$

$$I(0,t) = \begin{cases} I_0; t \leq t_2 \\ I_1; t_2 < t \leq t_{31} \\ I_i; t_{3(i-1)} < t \leq t_{3i} \end{cases}, i = 1, 2, 3, \ldots. \tag{11}$$

$$c(0,t) = \begin{cases} c_0; t \leq t_1 \\ 0; t > t_1 \end{cases} \tag{12}$$

$$\left.\frac{\partial I}{\partial z}\right|_{(L,t)} = \left.\frac{\partial c}{\partial z}\right|_{(L,t)} = 0 \tag{13}$$

Here, I_0 is the initial value of ionic strength of the background electrolyte in the soil before starting colloid transport experiments, t_1 is the duration of injection of colloidal suspension at the inlet of the column in stage 1, t_2 is time till the end of stage 2, I_1 is the ionic strength at the column inlet for first step decrease in ionic strength at the start of stage 3, t_{31} is the time till the end of first step decrease in ionic strength, I_i is the ionic strength at the column inlet for i^{th} step-decrease in ionic strength in stage 3, t_{3i} is the time till the end of i^{th} step decrease in ionic strength, and i is the number of steps of ionic strength reduction. Eq. (10) indicates that the initial value of ionic strength in the liquid phase was I_0, and there were no colloids present in the liquid and solid phases initially. The governing Eqs. (2)–(9), subject to the initial and boundary conditions (Eqs. (10)–(13)), were solved numerically using COMSOL Multiphysics software (version 5.5). There may be many other mechanisms influencing the colloid release that are not included here. Doing so would require many more data for evaluating the model. For example, a relevant mechanism is release of attached colloids as aggregates after sudden changes in ionic strength and their subsequent straining in the downstream pores. The model performance could be improved by including aggregation kinetics and straining during the release. However, including such a mechanism in the model will be useful only if data required for evaluating corresponding parameters is available.

3.2. Fitting procedure

The model contains (Eqs. (2)–(9)) eight unknown parameters (D_L, f, k_D, k_a, k_d, k'_{d_0}, I_c and β) whose values were estimated by fitting different stages of the tracer and colloid transport breakthrough curves as explained below. First, the dispersion coefficient, D_L, was estimated by fitting the tracer breakthrough data with advection-dispersion equation. Colloids were assumed to have the same dispersivity as that of the tracer. Colloid dispersivity has been found to be size dependent (Chrysikopoulos and Katzourakis, 2015) and can be different from the dispersivity of tracer. Chrysikopoulos and Katzourakis (2015) observed a positive correlation between colloid dispersivity and its size. However, for simplicity we have assumed the dispersivity of colloid to be the same as that of the tracer. As a result, the dispersivity of colloids may be underestimated in this work. The value of f at a given ionic strength was estimated as the fraction of injected colloids recovered in the effluent in steady state stages 1 and 2 of experiments 1–7. This is reasonable as the value of detachment rate coefficient at the kinetic site during stages 1 and 2 is negligibly small. Then, the colloid breakthrough curve from stages 1 and 2 of experiments 1–7 were fitted with Eq. (3)–(4) to estimate the values of k_D, k_a, and k_d at different ionic strengths. This resulted in a list of values of k_D, k_a, and k_d at different values of ionic strengths. These values were then fitted with Eqs. (6)–(9), respectively, to estimate the values of a_i, b_i, d_j, and e_j where $i = 1, 2, 3$ and $j = 1, 2$. Following this step, colloid breakthrough curve from stage 3 of experiment 1 was fitted with Eqs. (3)–(5) to estimate the values of k'_{d_0}, I_c and β. Since k'_{d_0}, I_c and β are constant for a given combination of colloid type, soil type and hydraulic conditions, the estimated values of these parameters from experiment 1 were then used to simulate the breakthrough curves in stage 3 of experiments 2–4.

4. Results and discussion

4.1. Interaction energy profile

The zeta potentials of CML colloids and sand at various ionic

strengths and the corresponding depths and distances of primary and secondary minima are given in Table 2. Fig. 1 shows the interaction energy profile between CML colloids and grain surface at different ionic strengths. There, h [L] is the separation distance between colloid and grain surface, and a [L] is the colloid radius. The interaction energy profile at 100 mM is characterized by a deep primary minimum with a negligible energy barrier (Fig. 1), and hence, the conditions at 100 mM were favourable for deposition. At other ionic strengths, energy profiles are characterized by a secondary minimum and an energy barrier (Fig. 1 and Table 2), indicating unfavourable conditions for deposition. The depth of the secondary minimum increased from 0.00013 k_BT to 9.71 k_BT as ionic strength increased from 0.1 mM to 100 mM (Table 2), thereby increasing the potential for colloid retention at secondary minimum.

4.2. Colloid deposition during steady-state ionic strength (stages 1 and 2 of column experiments)

Experimental and model-fitted breakthrough curves of colloids at various ionic strengths (100, 50, 25, 10, 1, 0.1 mM, and DI water) during stages 1 and 2 of column experiments are given in Fig. 2. The developed model fitted the experimental breakthrough curves reasonably well (Fig. 2). The experimental mass balance information and the values of fitted parameters are given in Table 3. It is clear from Fig. 2 and Table 3 that colloid retention in soil increased with increasing ionic strength. This can be attributed to deeper secondary minimum at higher ionic strengths (Table 2). These findings are in line with the estimated values of k_a and k_d, which showed increasing and decreasing trends, respectively, with increasing ionic strength as given in Table 3. The fraction of equilibrium sites increased with decreasing ionic strength (Table 3). The estimated values of f, k_D, k_a and k_d were then used to find values of constants in Eqs. (6)–(9) that relate these parameters to ionic strength. The resulting values are reported in Table 4.

4.3. Colloid release during transients in ionic strength (stage 3 of column experiments)

Figs. 3 to 6 show the colloid release curves during stage 3 of column experiments 1 to 4, respectively. Colloid release curves during transients in ionic strength are characterized by sharp peaks followed by long tails, with the time to peak coinciding with the time of arrival of the ionic strength front at the column outlet (Figs. 3-6). This is in line with the observations reported in literature for CML colloids (Bradford and Kim, 2012; Bradford et al., 2015; Torkzaban et al., 2010; Tosco et al., 2009). It can also be seen from Figs. 3-6 that the amount of spike release during a given step-decrease in ionic strength in stage 3 depends on the history of colloid deposition and release. Significant spike release of deposited colloids was observed only at the step when ionic strength was decreased from 10 mM to 1 mM and smaller (Table 3). This could be due to the release of attached colloids from the tips of asperities at lower ionic strengths (Shen et al., 2018). This indicates that there may exist a critical ionic strength between 10 and 1 mM below which the spike release is significant as no significant release of colloids was observed at the previous step-decrease of ionic strength, i.e., 10 mM (Tosco et al., 2009). However, for all transient experiments, significant mass was still retained in the soil even after several steps of ionic strength transients. This indicates that only a fraction of the retained colloids on soil grains can be remobilized by ionic strength variations. Moreover, the fraction of retained colloids released during transients (stage 3) became smaller with larger value of ionic strength in stages 1 and 2 (Table 3). Similar observations have been reported by other authors (Pazmino et al., 2014; Torkzaban et al., 2010). The incomplete colloid release during transients may be due to the roughness on the grain surfaces (Shen et al., 2018; Wang et al., 2020) and colloid retention in low velocity regions such as grain to grain contact points and their subsequent aggregation there (Torkzaban et al., 2010). Rough collector surfaces may have depressions that act as favourable locations for colloid deposition. The colloids deposited in such depressions remain irreversibly deposited (Li et al., 2017; Shen et al., 2007). The long tail in the breakthrough curves after the passage of the ionic strength front was due to the slow detachment from the soil surface. This behavior was also reported in previous studies (Bradford et al., 2015; Lenhart and Saiers, 2003; Wang et al., 2020).

Fig. 3 shows that the developed model fitted the full breakthrough curve of experiment 1 (100 mM and subsequent decreases in ionic strength) reasonably well. The model-fitted parameter values for the transient release of colloids are $k'_{d_0} = 0.006\ \text{min}^{-1}$, $I_c = 7.48$ mM, and $\beta = 4.3$. This is in line with the experimental data (Figs. 3-6) which shows that significant spike release of colloids occur only when the ionic strength becomes smaller than 10 mM. Since the physicochemical conditions for experiments 1 to 4 were all the same, except for ionic strength, k'_{d_0}, I_c, and β are expected to remain the same for all four experiments. Hence, the model fitted parameter values of k'_{d_0}, I_c, and β obtained from experiment 1 (100 mM) were used to simulate the breakthrough curves for experiments 2–4. Figs. 4-6 show that the simulated curves match the full breakthrough curves, including spikes, for experiments 2 and 4 (Figs. 4 and 6), whereas there is some mismatch between the simulated and experimental breakthrough curves for experiment 3 (Fig. 5). Of course, one can improve the quality of fitting for all experiments by selecting different set of values for k'_{d_0}, I_c, and β for each experiment. Such an approach leads to four different sets of k'_{d_0}, I_c, and β values for the same soil; this is physically not acceptable. Also, unlike some of the existing models in the literature, where colloid release function changes with change in the boundary conditions (Bradford et al., 2015), the model developed in this study employs the same set of governing equations for stages 1, 2 and 3, which is physically correct. However, the model developed in this study did not capture the gradual release of colloids in the breakthrough curves after the passage of ionic strength front (Figs. 3-6).

The performance of the developed model in this study is comparable to existing models in the literature. For example, Lenhart and Saiers (2003) developed a mathematical model to simulate the release of colloids by dividing the immobile phase colloid population into a series of compartments. Colloid release from each compartment occurs when the ionic strength becomes lower than a critical value of solute

Table 2
Measured zeta potentials, primary and secondary minima depths and corresponding distances for CML colloid-sand interaction at various ionic strengths.

IS (mM)	Zeta potential of sand, ψ_2 (mV)[a]	Zeta potential of colloid, ψ_1(mV) [a]	Primary minimum		Secondary minimum	
			Depth (k_BT)	Distance from the grain surface (nm)	Depth (k_BT)	Distance from the grain surface (nm)
100	−13.08 (1.61)	−16.46 (0.39)	−109.51	0.3	−9.71	3.5
50	−16.03 (3.35)	−41.16 (0.68)	–	–	−3.09	9
25	−20.03 (3.76)	−45.35 (1.06)	–	–	−1.36	15.5
10	−29.57 (2.42)	−48.95 (0.66)	–	–	−0.45	29.5
1	−30.36 (0.69)	−67.46 (0.96)	–	–	−0.026	125
0.1	−31.01 (1.82)	−78.66 (3.04)	–	–	−0.00013	500
DI	−44.46 (2.97)	−84.15 (3.64)	–	–	–	–

[a] The values within the brackets represent the standard errors of zeta potential measurements.

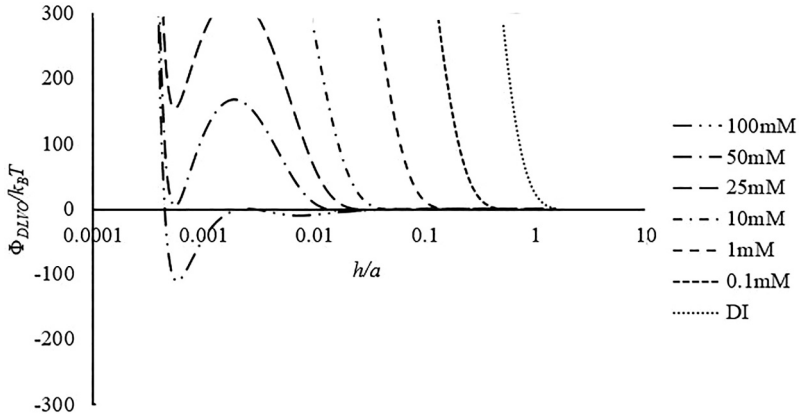

Fig. 1. DLVO energy profiles for the interaction of CML colloids with sand surface at various ionic strengths.

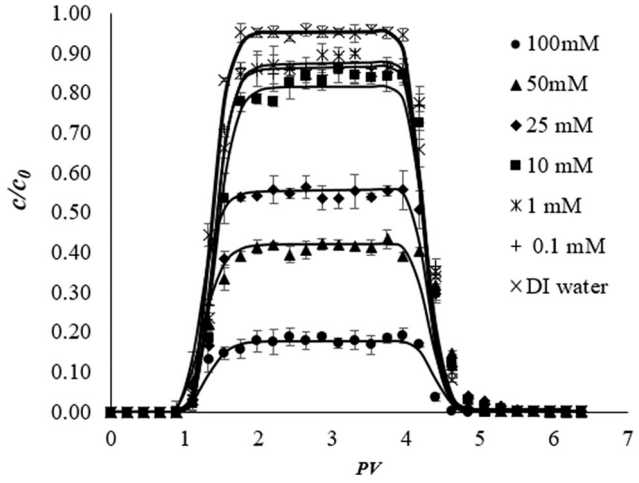

Fig. 2. Colloid breakthrough curves during stages 1 and 2 at various ionic strengths. The black continuous line represents the modelled breakthrough curve.

concentration. The model-fitted parameters for release of colloids caused by step decreases in ionic strength from 100 mM to 0 mM were used to simulate the release for step decreases in ionic strength from 40 mM to 0 mM and 10 mM to 0 mM. The model predicted the release spikes for 40 mM initial ionic strength well, but the decline in concentrations after the peak was overestimated. Also, the model performance was poorer for 10 mM initial ionic strength where the release spike was overestimated.

Fig. 7 shows the colloid retention profile at various stages for an initial ionic strength of 50 mM: at the end of stage 2 (experiment 8a), at the end of step decreases in ionic strength to 1 mM (experiment 8b), and at the end of step decreases in ionic strength to 0.1 mM (experiment 8c). Table 5 shows the mass balance information for experiments 8a-c. It is evident from Fig. 7 that colloid retention is more near the inlet than the outlet for all three experiments, indicating strong attachment to grain surfaces. Fig. 7 shows that colloid release from grain surfaces during step decreases in ionic strength to 1 mM (experiment 8b) mainly happens in the downstream part of the column. However, colloid release mainly occurs near to the column inlet for step decrease in ionic strength from 1 mM to 0.1 mM (experiment 8c). Also, the retention at the end of 0.1 mM (experiment 8c) is smaller than that at the end of 1 mM (experiment 8b). Significant amount of colloidal mass was still retained at the end of 0.1 mM ionic strength (experiment 8c and Table 5), which is in line with the observations based on colloid breakthrough curve in experiment 2 (Table 3). Fig. 7 also indicates that there might be straining of colloids happening in the initial part of the column during ionic strength transients. This may be because of the release of attached colloids in the form of aggregates from grain surfaces.

4.4. Factors affecting colloid release behavior

The discrepancy between the simulated and experimental breakthrough curves in this study (Figs. 3-5) can be attributed to mechanisms that could not be quantified in our measurements and therefore, are not included in our model. Among such mechanisms are: surface roughness of soil grains, irreversible deposition at stagnation zones of soil grains, and deposited colloids getting released as aggregates from the grain surface which were eventually strained downstream. Each of these mechanisms is discussed in detail in the following sections.

4.4.1. Roughness of soil grain surfaces

Colloid retention to and release from soil grains depends on the interaction energy between them. Though the interaction energy profile based on DLVO theory (Fig. 1) showed that the conditions were unfavourable for deposition at all ionic strengths except at 100 mM, experimental results showed strong kinetic deposition behavior at all ionic strengths (Fig. 2 and Table 3). This could be due to the surface roughness of the sand grains as classical DLVO theory assumes that colloid and soil grains are smooth and chemically homogeneous (Shen et al., 2011). But several studies have found that grain surfaces are rough, characterized by microscale asperities and depressions (Li et al., 2017; Liang et al., 2020; Shen et al., 2012; Shen et al., 2018; Wang et al., 2019). Surface roughness has been found to affect the interaction energy of colloids with grain surface by decreasing the energy barrier and primary minimum depth at the tip of the asperities, thereby making it less favourable for deposition (Pazmino et al., 2014; Shen et al., 2012; Shen et al., 2018; Wang et al., 2019). In contrast, depressions present between the roughness asperities were found to act as permanent retention sites for colloids (Li et al., 2017; Wang et al., 2019), which is the possible reason for the strong kinetic behavior with long tailing observed in this study.

According to the DLVO energy profile (Fig. 1 and Table 2), the secondary minimum is eliminated between 10 and 1 mM, and hence, all attached colloids were expected to get released when ionic strength was reduced to 1 mM and smaller. In contrast to this, the experimental data shows that only a fraction of the attached colloids on the grain surfaces were released during transients in ionic strength. One possible explanation for this observation is the strong attachment of colloids in the depressions of grain surfaces, which could not be released by ionic strength transients. This is in line with the results of Shen et al. (2012), Li et al. (2017), and Wang et al. (2019); they found that reduction in ionic strength caused the release of attached colloids from the tips of asperities whereas the colloids residing in the depressions were irreversibly attached.

Table 3
Experimental mass balance information and fitted model parameters.

Experiement No.	Stages 1 and 2							Stage 3								
	Ionic strength (mM)	M_{eluted} [a] (%)	$M_{retained}$ [b] (%)	f	k_D (cm^3/g)	k_a (min^{-1})	k_d (min^{-1})	R^2	Step 1	Step 2	Step 3	Step 4	Step 5	Step 6	Total M_{eluted} [c] (%)	Total $M_{retained}$ [d] (%)	R^2
1	100	17.81	82.19	0.18	0.397	0.078	0.00001	0.94	0.01	0.02	0.53	7.27	6.83	4.60	19.26	62.93	0.80
2	50	42.98	57.02	0.43	0.243	0.056	0.00003	0.99	0.52	1.61	8.15	6.35	4.76	–	21.38	35.64	0.74
3	25	54.52	45.48	0.54	0.185	0.048	0.00013	0.99	1.24	7.24	12.06	8.33	–	–	28.87	16.51	0.16
4	10	78.54	21.46	0.79	0.12	0.035	0.00028	0.98	1.84	2.56	1.37	–	–	–	5.77	15.68	0.66
5	1	83.63	16.37	0.84	0.108	0.031	0.00039	0.99	–	–	–	–	–	–	–	–	–
6	0.1	83.75	16.25	0.84	0.105	0.034	0.00040	0.99	–	–	–	–	–	–	–	–	–
7	0	92.59	7.41	0.90	0.096	0.019	0.00045	0.99	–	–	–	–	–	–	–	–	–

[a] Percentage mass eluted during stages 1 and 2.
[b] Percentage mass retained inside the column at the end of stage 2.
[c] Percentage mass eluted during stage 3.
[d] Percentage mass retained inside the column at the end of stage 3.

Table 4
Values of coefficients in Eqs. (6) to (9).

Coefficient	Equation no.	Value
a_1	6	10^{-6}
a_2	6	0.003
a_3	6	0.103
b_1	7	-9×10^{-7}
b_2	7	6×10^{-4}
b_3	7	0.03
d_1	8	4×10^{-4}
d_2	8	−0.04
e_1	9	0.86
e_2	9	−0.02

4.4.2. Retention in flow stagnation zones

Nishad et al. (2021) observed from micromodel experiments that colloids were predominantly deposited in flow stagnation zones under unfavourable conditions due to negligible fluid drag forces, and were not released during perturbations in ionic strength. This can also be a reason for the partial release of deposited colloids during transients observed in this study. Similar observations as in this study were reported by Bhuvankar et al. (2022) for the remobilization of clay colloids through pore-scale simulations. They found that temporal decrease in ionic strength led to lesser remobilization of clay particles when they were deposited at high ionic strengths. This was because at higher ionic strengths, clay particles got aggregated and remained attached in the downstream low velocity regions. Decrease in ionic strength resulted in the attached clay particles getting released as clusters, which may subsequently be strained in the downstream pores. Similar observations were reported by Torkzaban et al. (2010) from micromodel experiments when colloids were deposited at an ionic strength of 106 mM and then released by decreasing the ionic strength in a stepwise manner from 106 mM to DI water. They observed uniform distribution of colloids on the grain surface at all ionic strengths when ionic strength was reduced from 106 mM to 6 mM. However, aggregation of trapped colloids in low-velocity regions at grain-grain points was observed when ionic strength was decreased to DI water. The incomplete mass recovery was attributed to the formation of aggregates and funneling of colloids in low-velocity regions at grain-grain contacts. This may be another reason for the partial release of retained colloids observed in this study even after several steps of ionic strength decrease.

4.4.3. Straining of released aggregates

The discrepancy between the model output and the experimental data may be partly due to the release of colloids in the form of aggregates from the grain surface during decrease in ionic strength and their subsequent straining in the downstream pores (Liang et al., 2019). This mechanism may be prominent for experiments with high ionic strength in stages 1 and 2, where greater number of colloids was attached to the grain surface, and colloid-colloid interaction was more favourable. As a result, colloids deposited at higher ionic strengths detach as clusters from the grain surface during stage 3, and may get strained in the downstream pores (Bhuvankar et al., 2022; Nishad and Al-Raoush, 2021; Torkzaban et al., 2010). This is supported by Table 3 which shows only partial release of retained colloids even after several step-reductions in ionic strength, with the total release being smaller for experiments with high ionic strengths in stages 1 and 2. Also, the shape of the retention profile during stage 3 shown in Fig. 7 indicates that there may be straining near to the column inlet. Figs. 3-6 show extended tailing during colloid release, with the tailing more prevalent for higher ionic strength experiments in stages 1 and 2 (experiments 1 and 2). This is because of the difference in the transport behavior of individual colloids and the aggregates. Aggregation of colloidal particles during transients in ionic strength was also reported by Zhou et al. (2011).

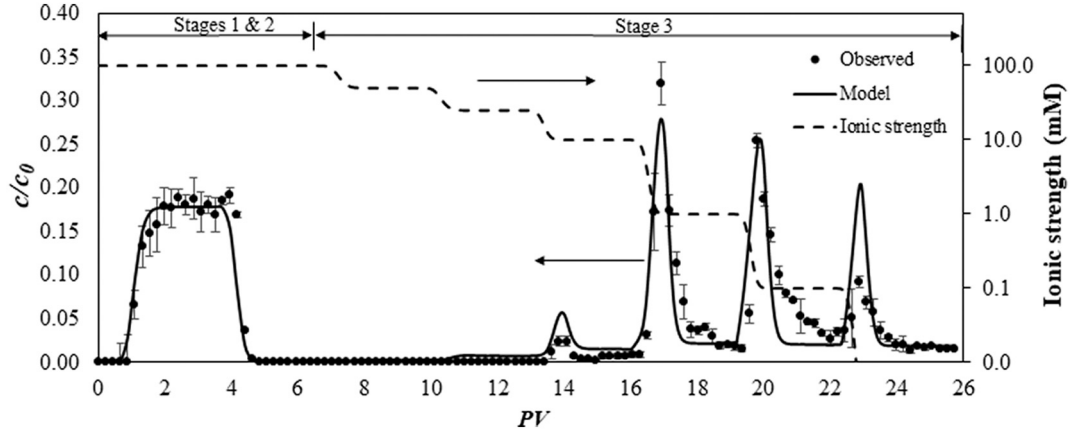

Fig. 3. Observed and fitted breakthrough curves of CML colloids for experiment 1. Simulated ionic strength at the outlet is shown on the secondary y-axis.

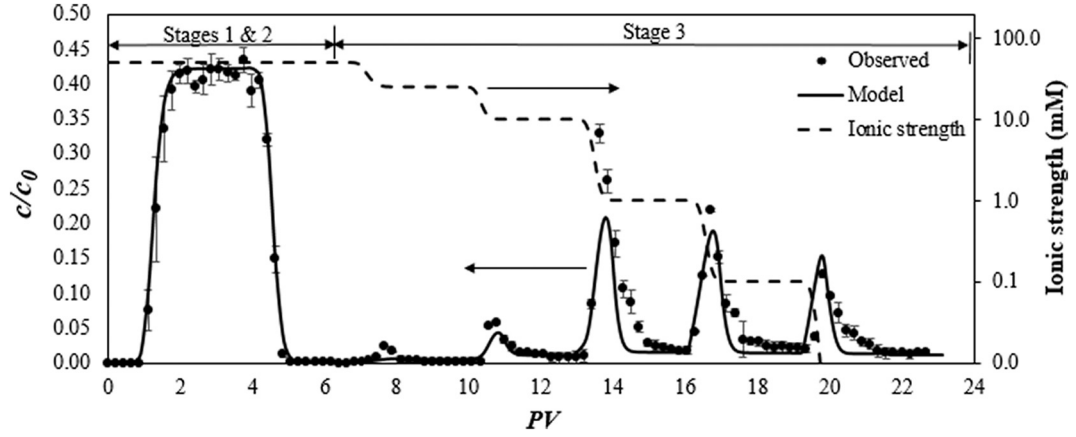

Fig. 4. Observed and simulated breakthrough curves of CML colloids for experiment 2. Simulated ionic strength at the outlet is shown on the secondary y-axis.

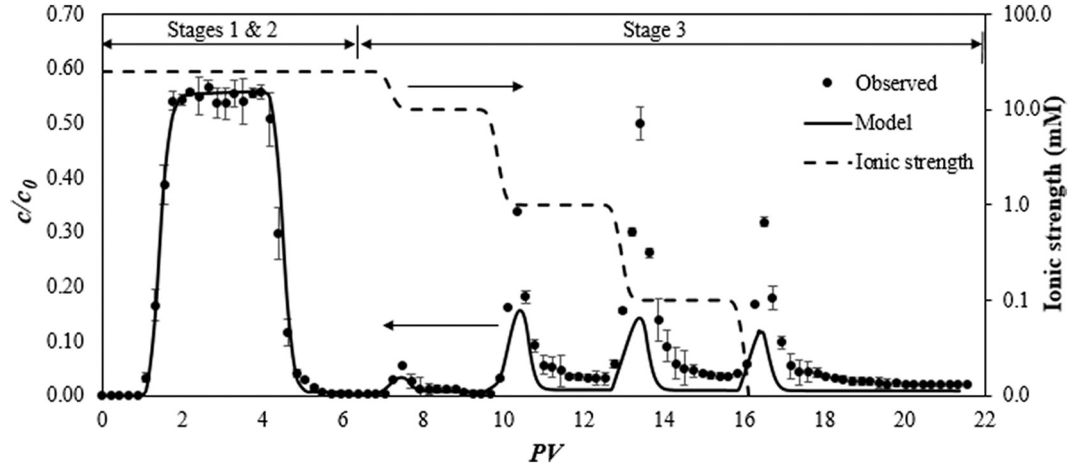

Fig. 5. Observed and simulated breakthrough curves of CML colloids for experiment 3. Simulated ionic strength at the outlet is shown on the secondary y-axis.

5. Summary and conclusions

There are only limited studies on the effect of sudden changes in water chemistry on transport of colloids in porous media. Also, the reported laboratory experiments and proposed models do not seem to be applicable for a wide range of conditions. We have performed a systematic study of the effect of temporal variations in ionic strength on colloid remobilization and re-deposition in porous media under saturated conditions. This was done by performing four sets of column experiments, each at a different value of initial ionic strength (100, 50, 25 and 10 mM) followed by stepwise reduction of the inflow solution ionic strength to 0 mM. We observed a sharp spike followed by a long tail in the effluent colloid concentration for every step-decrease in ionic strength, with the peak value being significantly higher when ionic strength becomes smaller than 10 mM. Also, our experimental results show that only a fraction of the retained colloids was mobilized during

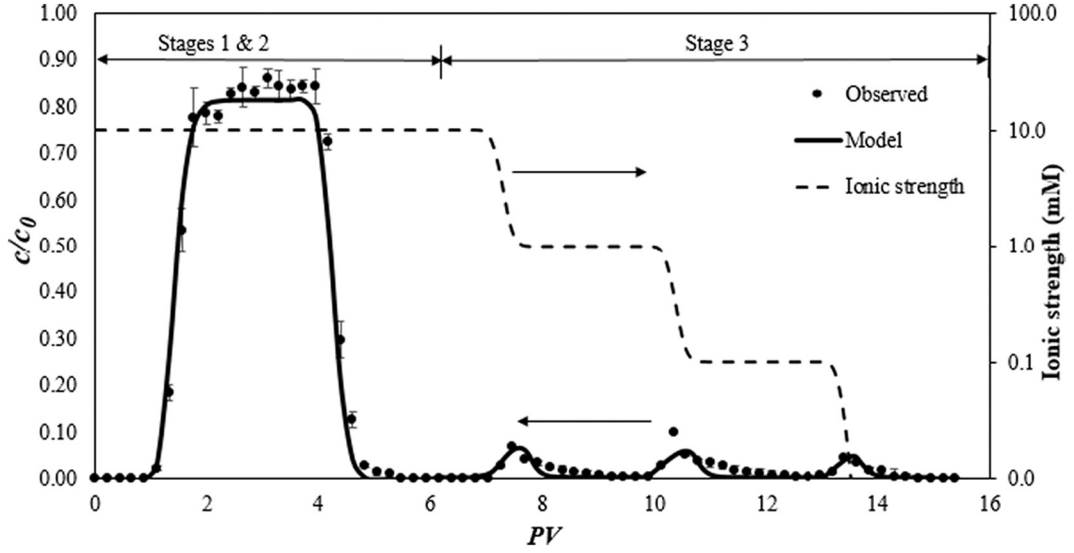

Fig. 6. Observed and simulated breakthrough curves of CML colloids for experiment 4. Simulated ionic strength at the outlet is shown on the secondary y-axis.

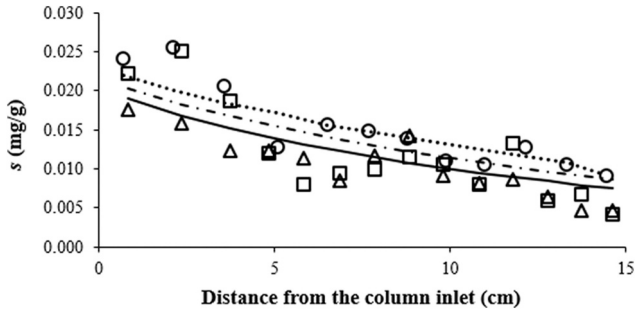

Fig. 7. Colloid retention profile in the soil at various stages for an initial ionic strength of 50 mM: at the end of stage 2 (experiment: ○, model: ·····), at the end of step decrease in ionic strength to 1 mM (experiment: □, model: – · –), and at the end of step decrease in ionic strength to 0.1 mM (experiment: △, model: ——).

Table 5
Mass balance information for experiments performed to measure colloid retention profile.

Experiment	M_{eluted}[a] (%)		$M_{retained}$[b] (%)	$M_{recovered}$[c] (%)
	Stages 1 and 2	Stage 3		
8a	44.35 (44.94)	–	55.36 (53.33)	99.70 (98.27)
8b	43.07 (44.94)	10.27 (5.8)	45.83 (49.70)	99.17 (99.94)
8c	43.30 (44.94)	16.40 (10)	39.88 (44.63)	99.58 (99.57)

[a] Percentage mass eluted in the experiments. The values in the brackets represent the mass eluted calculated from the modelled curves.

[b] Percentage mass retained inside the column at the end of stage 2 (experiment 8a) and stage 3 (experiments 8b&c) calculated from the experimental retention profile. The values in the brackets represent the mass retained calculated from the modelled curves.

[c] Percentage mass recovered from the experiments calculated as the sum of percentage mass eluted and percentage mass retained. The values in the brackets represent the mass recovered from the modelled curves calculated as the sum of percentage mass eluted and percentage mass retained.

ionic strength transients, and the fraction of remobilized colloids was smaller for higher value of initial ionic strength of inflow water. Further, experimental results were numerically simulated using a mathematical model containing a novel formulation for ionic-strength dependent colloid attachment and release rate coefficients. Since significant release of colloids was only observed for ionic strength reduction below 10 mM, it was assumed in the model that there is a critical concentration of ionic strength below which colloid release is fast. The estimated value of the critical ionic strength was 7.48 mM. The same set of model parameter values were used to simulate the colloid breakthrough curves obtained from all four sets of column experiments. The model output was found to match the spikes in the colloid release curves of the experimental data reasonably well for initial ionic strengths of 100 mM, 50 mM and 10 mM. However, the model did not capture well the descending part of the release curves for all initial ionic strengths and also the peaks in the release curve for initial ionic strength of 25 mM. It may be mentioned that we could obtain a good fit between our simulations and experimental release curve for initial ionic strength of 25 mM by simply varying the values of model parameters, as done in some other models. That, however, we do not find satisfactory. The discrepancy in the model output and experimental results may be due to mechanisms which were not considered in the model. Potential mechanisms include surface roughness of soil grains, retention of colloids in low-velocity regions, and detachment of retained colloids as aggregates and their subsequent straining in the downstream pores. Though colloid retention profile during temporal reduction in ionic strength indicates that there may be straining of colloids near the column inlet, further research is needed, especially at the pore scale, to elucidate the detachment mechanisms, and thereby to improve the performance of developed mathematical model.

CRediT authorship contribution statement

Yerramilli Sai Rama Krishna: Conceptualization, Methodology, Investigation, Formal analysis, Writing – original draft. **N. Seetha:** Conceptualization, Methodology, Supervision, Writing – review & editing. **S. Majid Hassanizadeh:** Conceptualization, Writing – review & editing.

Declaration of Competing Interest

The authors declare that they have no known competing financial interests or personal relationships that could have appeared to influence the work reported in this paper.

Acknowledgements

The authors acknowledge the funding received from Science and Engineering Research Board (SERB), Government of India (sanction no. VJR/2020/000006) for carrying out this work. SMH acknowledges support form Deutsche Forschungsgemeinschaft (DFG, German Research Foundation) under Germany's Excellence Strategy - EXC 2075-390740016 and from the Stuttgart Center for Simulation Science (SimTech). The authors also thank the anonymous reviewers for their valuable comments which helped to improve the manuscript.

Appendix A. Appendix

A.1. Determining the metal contents on sand surface using inductively coupled plasma mass spectrometry (ICPMS)

The sand samples were digested in 1:4 ratio of HCl: HNO_3 in a microwave digester to dissolve the metals from the sand surface (Carter and Gregorich, 2007). The supernatant was then decanted and analyzed for different metals. Sodium, calcium, magnesium, aluminum, and iron were the major metals present on the sand whereas nickel, copper, zinc, chromium, and manganese were present in minor quantities before acid washing. Acid treatment led to the complete removal of calcium, nickel, copper, zinc, and chromium. Sodium and magnesium concentrations were found to be 255.84 μg/g and 189.48 μg/g, respectively, in the acid washed sand with removal efficiencies of 87% and 90%. Aluminum, being the constituent of sand, was still detected in acid treated sand having a concentration of 1177.30 μg/g, exhibiting a removal efficiency of 80%. The concentrations of manganese and iron after acid washing were 5.3 μg/g and 145.84 μg/g, respectively, with a removal efficiency of 97% for both of them.

A.2. Interaction energy calculations

The van der Waals energy was calculated using the following expressions given by Gregory (1981) and Weroński and Elimelech (2008) (see also Seetha et al., 2015):

$$\frac{\Phi_{vdW}}{k_BT} = \frac{-aH}{6hk_BT}\left[1 + \left(\frac{14h}{\lambda}\right)\right]^{-1}; h \le 0.2a \tag{A-1a}$$

$$\frac{\Phi_{vdW}}{k_BT} = \frac{-H}{6k_BT}\left[\frac{2.45\lambda}{10\pi}\left(\frac{a-h}{h^2} + \frac{3a+h}{(2a+h)^2}\right) - \frac{2.17\lambda^2}{120\pi^2}\left(\frac{2a-h}{h^3} + \frac{4a+h}{(2a+h)^3}\right) + \frac{0.59\lambda^3}{840\pi^3}\left(\frac{3a-h}{h^4} + \frac{5a+h}{(2a+h)^4}\right)\right]; h > 0.2a \tag{A-1b}$$

Here, H [ML^2T^{-2}] is the Hamaker constant and λ [L] is the characteristic wavelength of interaction taken as 100 nm.

The electrostatic double-layer energy was calculated using the expression given by Hogg-Healy-Fuerstenau expression (Hogg et al., 1966) as

$$\frac{\Phi_{EDL}}{k_BT} = \frac{\pi\varepsilon\varepsilon_0 a}{k_BT}\left[2\psi_1\psi_2\, ln\left(\frac{1+e^{-(\kappa h)}}{1-e^{-(\kappa h)}}\right) + \left(\psi_1{}^2 + \psi_2{}^2\right) ln\left(1-e^{-(2\kappa h)}\right)\right] \tag{A-2}$$

Here, ε [−] is the dielectric constant of water, ε_0 [$ML^{-3}T^4I^2$] is the permittivity of vacuum (equal to 8.854×10^{-12} C^2J^{-1} m^{-1}), a [L] is the colloid radius, ψ_1[$ML^2T^{-3}A^{-1}$] and ψ_2 [$ML^2T^{-3}A^{-1}$] are the surface potentials of colloids and the sand grains, respectively, κ [L^{-1}] is the inverse Debye length given by the expression $\kappa = \sqrt{2000\, N_A I e^2/\varepsilon\varepsilon_0 k_B T}$, N_A [−] is the Avogadro number, I [Molar] is the ionic strength, e [T^1I^1] is the elementary charge of the particle, and h [L] is the separation distance between colloid and grain surface.

Born repulsion energy was calculated using the expression given by Ruckenstein and Prieve (1976):

$$\frac{\Phi_{Born}}{k_BT} = \frac{H(\sigma)^6}{7560k_BT}\left[\frac{8a+h}{(2a+h)^7} - \frac{6a-h}{(h)^7}\right] \tag{A-3}$$

where, σ is the collision diameter assumed to be 0.5 nm (Ruckenstein and Prieve, 1976).

References

Bales, R.C., Li, S., Yeh, T.C.J., Lenczewski, M.E., Gerba, C.P., 1997. Bacteriophage and microsphere transport in saturated porous media: forced-gradient experiment at Borden, Ontario. Water Resour. Res. 33 (4), 639–648.

Bergendahl, J., Grasso, D., 1999. Prediction of colloid detachment in a model porous media: thermodynamics. AICHE J. 45 (3), 475–484. https://doi.org/10.1002/aic.690450305.

Bhuvankar, P., Cihan, A., Birkholzer, J., 2022. Pore-scale CFD simulations of clay mobilization in natural porous media due to fresh water injection. Chem. Eng. Sci. 247 https://doi.org/10.1016/j.ces.2021.117046.

Bradford, S.A., Bettahar, M.E.H.D.I., 2005. Straining, attachment, and detachment of Cryptosporidium oocysts in saturated porous media. J. Environ. Qual. 34 (2), 469–478.

Bradford, S.A., Kim, H., 2012. Causes and implications of colloid and microorganism retention hysteresis. J. Contam. Hydrol. 138–139, 83–92. https://doi.org/10.1016/j.jconhyd.2012.06.007.

Bradford, S.A., Torkzaban, S., Walker, S.L., 2007. Coupling of physical and chemical mechanisms of colloid straining in saturated porous media. Water Res. 41 (13), 3012–3024.

Bradford, S.A., Torkzaban, S., Kim, H., Simunek, J., 2012. Modeling colloid and microorganism transport and release with transients in solution ionic strength, 48 (May), 1–10. https://doi.org/10.1029/2012WR012468.

Bradford, S.A., Torkzaban, S., Leij, F., Simunek, J., 2015. Equilibrium and kinetic models for colloid release under transient solution chemistry conditions. J. Contam. Hydrol. 181, 141–152. https://doi.org/10.1016/j.jconhyd.2015.04.003.

Bundschuh, M., Filser, J., Lüderwald, S., McKee, M.S., Metreveli, G., Schaumann, G.E., Schulz, R., Wagner, S., 2018. Nanoparticles in the environment: where do we come from, where do we go to? Environ. Sci. Eur. 30 (1) https://doi.org/10.1186/s12302-018-0132-6.

Carrard, N., Foster, T., Willetts, J., 2020. Correction: groundwater as a source of drinking water in southeast asia and the pacific: a multi-country review of current reliance and resource concerns. [water (2019), 11, (1605)]. Water (Switzerland) 12 (1). https://doi.org/10.3390/w12010298.

Carter, M.R., Gregorich, E.G. (Eds.), 2007. Soil Sampling and Methods of Analysis, 2nd ed. CRC Press. https://doi.org/10.1201/9781420005271.

Cheng, T., Saiers, J.E., 2009. Mobilization and transport of in situ colloids during drainage and imbibition of partially saturated sediments. Water Resour. Res. 45 (8), 1–14. https://doi.org/10.1029/2008WR007494.

Chrysikopoulos, C.V., Katzourakis, V.E., 2015. Colloid particle size-dependent dispersivity. Water Resour. Res. 51 (6), 4668–4683.

Chrysikopoulos, C.V., Syngouna, V.I., 2014. Effect of gravity on colloid transport through water-saturated columns packed with glass beads: modeling and experiments. Environ. Sci. Technol. 48 (12), 6805–6813.
Derjaguin, B.V., Landau, L.D., 1941. Theory of the stability of strongly charged lyophobic sols and the adhesion of strongly charged particles in solutions of electrolytes: acta Physicochim URSS, v. 14. In: Laboratory of Thin Films, and Instilute of Physical Problems, Moscow (Received 1941).
Elimelech, M., O'Melia, C.R., 1990. Kinetics of deposition of colloidal particles in porous media. Environ. Sci. Technol. 24 (10), 1528–1536. https://doi.org/10.1021/es00080a012.
Fang, J., Xu, M. Jia, Wang, D. Jun, Wen, B., Han, J. Yi, 2013. Modeling the transport of TiO2 nanoparticle aggregates in saturated and unsaturated granular media: effects of ionic strength and pH. Water Res. 47 (3), 1399–1408. https://doi.org/10.1016/j.watres.2012.12.005.
Gregory, J., 1981. Approximate expressions for retarded van der Waals interaction. J. Colloid Interface Sci. 83 (1), 138–145.
Hogg, R., Healy, T.W., Fuerstenau, D.W., 1966. Mutual coagulation of colloidal dispersions. Trans. Faraday Soc. 62 (615), 1638–1651. https://doi.org/10.1039/tf9666201638.
Johnson, W.P., Pazmino, E., Ma, H., 2010. Direct observations of colloid retention in granular media in the presence of energy barriers, and implications for inferred mechanisms from indirect observations. Water Res. 44 (4), 1158–1169. https://doi.org/10.1016/j.watres.2009.12.014.
Katzourakis, V.E., Chrysikopoulos, C.V., 2021. Modeling the transport of aggregating nanoparticles in porous media. Water Resour. Res. 57 (1), e2020WR027946.
Kohler, M., Curtis, G.P., Kent, D.B., Davis, J.A., 1996. Experimental investigation and modeling of uranium (VI) transport under variable chemical conditions. Water Resour. Res. 32 (12), 3539–3551.
Lenhart, J.J., Saiers, J.E., 2003. Colloid mobilization in water-saturated porous media under transient chemical conditions. Environ. Sci. Technol. 37 (12), 2780–2787. https://doi.org/10.1021/es025788v.
Li, X., Johnson, W.P., 2005. Nonmonotonic variations in deposition rate coefficients of microspheres in porous media under unfavorable deposition conditions. Environ. Sci. Technol. 39 (6), 1658–1665.
Li, T., Jin, Y., Huang, Y., Li, B., Shen, C., 2017. Observed dependence of colloid detachment on the concentration of initially attached colloids and collector surface heterogeneity in porous media. Environ. Sci. Technol. 51 (5), 2811–2820. https://doi.org/10.1021/acs.est.6b06264.
Liang, Y., Bradford, S.A., Šimůnek, J., Klumpp, E., 2019. Mechanisms of graphene oxide aggregation, retention, and release in quartz sand. Sci. Total Environ. 656, 70–79.
Liang, Y., Zhou, J., Dong, Y., Klumpp, E., Šimůnek, J., Bradford, S.A., 2020. Evidence for the critical role of nanoscale surface roughness on the retention and release of silver nanoparticles in porous media. Environ. Pollut. 258, 113803 https://doi.org/10.1016/j.envpol.2019.113803.
Nishad, S., Al-Raoush, R.I., 2021. Colloid retention and mobilization mechanisms under different physicochemical conditions in porous media: a micromodel study. Powder Technol. 377, 163–173. https://doi.org/10.1016/j.powtec.2020.08.086.
Nishad, S., Al-Raoush, R.I., Alazaiza, M.Y.D., 2021. Release of colloids in saturated porous media under transient hydro-chemical conditions: a pore-scale study. Colloids Surf. A Physicochem. Eng. Asp. 614 (December 2020) https://doi.org/10.1016/j.colsurfa.2021.126188.
Pazmino, E., Trauscht, J., Johnson, W.P., 2014. Release of colloids from primary minimum contact under unfavorable conditions by perturbations in ionic strength and flow rate. Environ. Sci. Technol. 48 (16), 9227–9235. https://doi.org/10.1021/es502503y.
Powelson, D.K., Gerba, C.P., Yahya, M.T., 1993. Virus transport and removal in wastewater during aquifer recharge. Water Res. 27 (4), 583–590. https://doi.org/10.1016/0043-1354(93)90167-G.
Ruckenstein, E., Prieve, D.C., 1976. Adsorption and desorption of particles and their chromatographic separation. AICHE J. 22 (2), 276–283. https://doi.org/10.1002/aic.690220209.
Ryan, J.N., Elimelech, M., 1996. Colloid mobilization and transport in groundwater. Colloids Surf. A Physicochem. Eng. Asp. 107, 1–56.
Sadeghi, G., Schijven, J.F., Behrends, T., Hassanizadeh, S.M., Gerritse, J., Kleingeld, P.J., 2011. Systematic study of effects of pH and ionic strength on attachment of phage PRD1. Ground Water 49 (1), 12–19. https://doi.org/10.1111/j.1745-6584.2010.00767.x.
Sadeghi, G., Behrends, T., Schijven, J.F., Hassanizadeh, S.M., 2013. Effect of dissolved calcium on the removal of bacteriophage PRD1 during soil passage: the role of double-layer interactions. J. Contam. Hydrol. 144 (1), 78–87. https://doi.org/10.1016/j.jconhyd.2012.10.006.
Sasidharan, S., Torkzaban, S., Bradford, S.A., Dillon, P.J., Cook, P.G., 2014. Coupled effects of hydrodynamic and solution chemistry on long-term nanoparticle transport and deposition in saturated porous media. Colloids Surf. A Physicochem. Eng. Asp. 457 (1), 169–179. https://doi.org/10.1016/j.colsurfa.2014.05.075.
Sasidharan, S., Torkzaban, S., Bradford, S.A., Cook, P.G., Gupta, V.V., 2017. Temperature dependency of virus and nanoparticle transport and retention in saturated porous media. J. Contam. Hydrol. 196, 10–20.
Shen, C., Li, B., Huang, Y., Jin, Y., 2007. Kinetics of coupled primary- and secondary-minimum deposition of colloids under unfavorable chemical conditions. Environ. Sci. Technol. 41 (20), 6976–6982. https://doi.org/10.1021/es070210c.
Shen, C., Li, B., Wang, C., Huang, Y., Jin, Y., 2011. Surface roughness effect on deposition of Nano- and Micro-sized colloids in saturated columns at different solution ionic strengths. Vadose Zone J. 10 (3), 1071–1081. https://doi.org/10.2136/vzj2011.0011.
Shen, C., Lazouskaya, V., Zhang, H., Wang, F., Li, B., Jin, Y., Huang, Y., 2012. Theoretical and experimental investigation of detachment of colloids from rough collector surfaces. Colloids Surf. A Physicochem. Eng. Asp. 410, 98–110. https://doi.org/10.1016/j.colsurfa.2012.06.025.
Seetha, N., Hassanizadeh, S.M., Mohan Kumar, M.S., Raoof, Amir, 2015. Correlation equations for average deposition rate coefficients of nanoparticles in a cylindrical pore. Water Resour. Res. 51 (10), 8034–8059. https://doi.org/10.1002/2015WR017723.
Shen, C., Bradford, S.A., Li, T., Li, B., Huang, Y., 2018. Can nanoscale surface charge heterogeneity really explain colloid detachment from primary minima upon reduction of solution ionic strength? J. Nanopart. Res. 20 (6) https://doi.org/10.1007/s11051-018-4265-8.
Syngouna, V.I., Chrysikopoulos, C.V., 2011. Transport of biocolloids in water saturated columns packed with sand: effect of grain size and pore water velocity. J. Contam. Hydrol. 126 (3–4), 301–314.
Tan, Y., Gannon, J.T., Baveye, P., Alexander, M., 1994. Transport of bacteria in an aquifer sand: experiments and model simulations. Water Resour. Res. 30 (12), 3243–3252.
Torkzaban, S., Bradford, S.A., Walker, S.L., 2007. Resolving the coupled effects of hydrodynamics and DLVO forces on colloid attachment in porous media. Langmuir 23 (19), 9652–9660. https://doi.org/10.1021/la700995e.
Torkzaban, S., Bradford, S.A., van Genuchten, M.T., Walker, S.L., 2008. Colloid transport in unsaturated porous media: the role of water content and ionic strength on particle straining. J. Contam. Hydrol. 96 (1–4), 113–127.
Torkzaban, S., Kim, H.N., Simunek, J., Bradford, S.A., 2010. Hysteresis of colloid retention and release in saturated porous media during transients in solution chemistry. Environ. Sci. Technol. 44 (5), 1662–1669. https://doi.org/10.1021/es903277p.
Torkzaban, S., Bradford, S.A., Vanderzalm, J.L., Patterson, B.M., Harris, B., Prommer, H., 2015. Colloid release and clogging in porous media: effects of solution ionic strength and flow velocity. J. Contam. Hydrol. 181, 161–171. https://doi.org/10.1016/j.jconhyd.2015.06.005.
Tosco, T., Tiraferri, A., Sethi, R., 2009. Ionic strength dependent transport of microparticles in saturated porous media: modeling mobilization and immobilization phenomena under transient chemical conditions. Environ. Sci. Technol. 43 (12), 4425–4431.
Treumann, S., Torkzaban, S., Bradford, S.A., Visalakshan, R.M., Page, D., 2014. An explanation for differences in the process of colloid adsorption in batch and column studies. J. Contam. Hydrol. 164, 219–229. https://doi.org/10.1016/j.jconhyd.2014.06.007.
Verwey, E.J.W., Overbeek, J.Th.G., 1948. Theory of the Stability of Lyophobic Colloids: The Interaction of sol Particles Having an Electric Double Layer. Elsevier, Amsterdam.
Wan, J., Wilson, J.L., 1994. Resources colloid transport in unsaturated porous media abstract. This paper explores of the gas-water interface sorption of polystyrene. Water Resour. Res. 30 (4).
Wang, C., Bobba, A.D., Attinti, R., Shen, C., Lazouskaya, V., Wang, L.P., Jin, Y., 2012. Retention and transport of silica nanoparticles in saturated porous media: effect of concentration and particle size. Environ. Sci. Technol. 46 (13), 7151–7158. https://doi.org/10.1021/es300314n.
Wang, Y., Bradford, S.A., Simunek, J., 2014. Release of *E. coli* D21g with transients in water content. Environ. Sci. Technol. 48 (16), 9349–9357. https://doi.org/10.1021/es501956k.
Wang, H., Zhang, W., Zeng, S., Shen, C., Jin, C., Huang, Y., 2019. Interactions between nanoparticles and fractal surfaces. Water Res. 151, 296–309. https://doi.org/10.1016/j.watres.2018.12.029.
Wang, Y., Bradford, S.A., Shang, J., 2020. Release of colloidal biochar during transient chemical conditions: the humic acid effect. Environ. Pollut. 260, 114068 https://doi.org/10.1016/j.envpol.2020.114068.
Weroński, P., Elimelech, M., 2008. Novel numerical method for calculating initial flux of colloid particle adsorption through an energy barrier. J. Colloid Interface Sci. 319 (2), 406–415. https://doi.org/10.1016/j.jcis.2007.10.042.
Zhou, Dongmei, Wang, Dengjun, Cang, Long, Hao, Xiuzhen, Chu, Lingyang, 2011. Transport and re-entrainment of soil colloids in saturated packed column: effects of pH and ionic strength. J. Soils Sediments 11, 491–503. https://doi.org/10.1007/s11368-010-0331-2.